Supplemental Materials: Effective spin-1 breathing kagome Hamiltonian induced by the exchange hierarchy in the maple leaf mineral bluebellite

Pratyay Ghosh,[1,2] Tobias Müller,[1] Yasir Iqbal,[3] Ronny Thomale,[1,3] and Harald O. Jeschke[4,3]

[1] *Institut für Theoretische Physik und Astrophysik and Würzburg-Dresden Cluster of Excellence ct.qmat, Julius-Maximilians-Universität Würzburg, Am Hubland Campus Süd, Würzburg 97074, Germany*
[2] *Institute of Physics, Ecole Polytechnique Fédérale de Lausanne (EPFL), CH-1015 Lausanne, Switzerland*
[3] *Department of Physics and Quantum Centers in Diamond and Emerging Materials (QuCenDiEM) group, Indian Institute of Technology Madras, Chennai 600036, India*
[4] *Research Institute for Interdisciplinary Science, Okayama University, Okayama 700-8530, Japan*

I. DETAILS OF ELECTRONIC STRUCTURE CALCULATIONS AND ENERGY MAPPING

Preparation of crystal structure.- The crystal structure of bluebellite $Cu_6IO_3(OH)_{10}Cl$ has been determined from mineral samples [1] and from synthetic polycrystals [2]. In the latter case, hydrogen positions were not determined. As the magnetic measurements were performed for synthetic bluebellite, it is necessary to prepare the crystal structure for electronic structure calculations and energy mapping by adding and optimizing hydrogen positions. Furthermore, Cl, O2 and H2 all have coordinates (0,0,z), restricting their position by symmetry to an axis, and H2 needs to be placed between Cl and O2, in accordance with the Mills *et al.* structure [1]. At a distance $d_{\mathrm{Cl-O2}} = 2.205\,\text{Å}$, there is insufficient space for an O2-H2 bond and a Cl-H hydrogen bond. Therefore, Cl and O2 positions need to be optimized as well. For consistency, we optimize all O positions as well. The resulting structure is given in Table S2.

DFT energy mapping.- We determine the Heisenberg Hamiltonian parameters of bluebellite by DFT energy mapping. For this purpose, we create a $\sqrt{2}\times\sqrt{2}\times 1$ supercell of the structure given in Table S2 with 12 symmetry inequivalent Cu^{2+} sites. This provides 948 distinct energies of spin configurations and allows us to resolve the first 20 nearest neighbor exchange paths which we name J_1 to J_{20}. We calculate 40 of these energies for five different values of the onsite interaction strength U; this provides us the five sets of exchange interactions given in Table S1 with statistical errors given in brackets. Slight extrapolation leads to the line in bold face that matches the experimental value of the Curie-Weiss temperature which we calculate according to

$$\theta_{\mathrm{CW}} = -\frac{1}{3}S(S+1)\big((J_1+J_2+J_3+J_4+J_5+J_6+J_7 + J_8+J_9+J_{10}+J_{11}+J_{12}+J_{13}+J_{14} + J_{15}+J_{16}+J_{17}+J_{18}+J_{19}+J_{20}\big) \tag{S1}$$

The couplings J_1 to J_5 are the nearest neighbor couplings making up the maple leaf lattice; they are by far the largest couplings in the model, and they are the main focus of our analysis. Couplings J_6 to J_{10} (for an illustration see Fig. 1**b** of the main text) as well as J_{15}, J_{16} and J_{18} to J_{20} are interlayer couplings. They are at most 10%

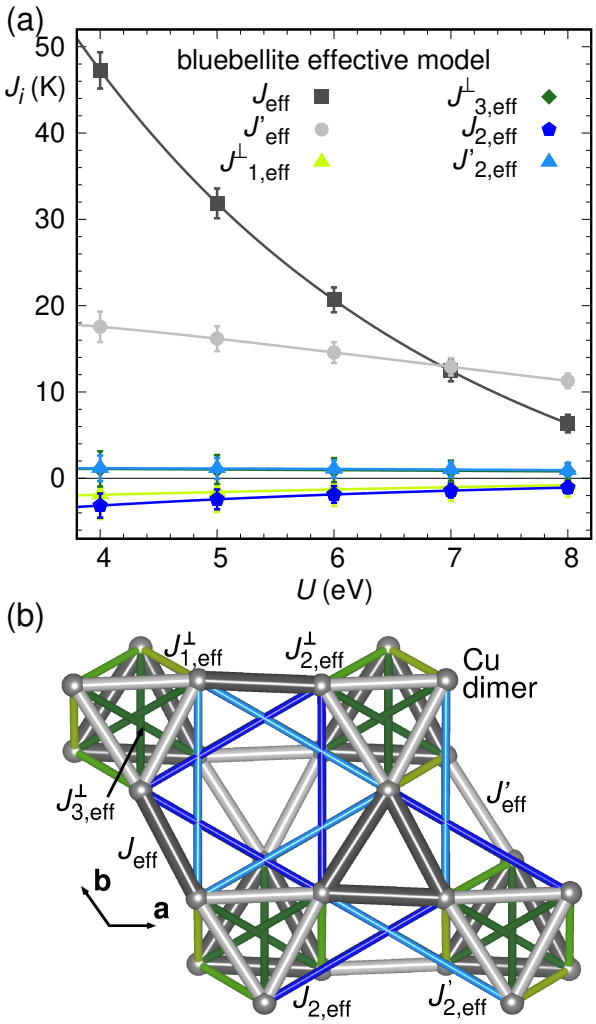

Figure S1. Energy mapping calculation for the effective spin-1 kagome lattice Hamiltonian. (a) Exchange interactions for five different values of on-site interaction U at fixed Hund's rule coupling strength J_{H}. (b) Exchange paths of the effective $S = 1$ lattice of bluebellite. Balls represent the Cu dimers of bluebellite with the strongest ferromagnetic coupling. J_{eff} and J'_{eff} correspond to small and large triangles in the breathing kagome network. Couplings marked "$\perp$" indicate interlayer couplings.

Table S1. Exchange interactions of bluebellite obtained by DFT energy mapping as described in the main text. The line in bold face corresponds to the set of couplings that match the experimental Curie-Weiss temperature [2].

U eV	J_1 (K)	J_2 (K)	J_3 (K)	J_4 (K)	J_5 (K)	J_6 (K)	J_7 (K)	J_8 (K)	J_9 (K)	J_{10} (K)	
3.9	**-120.8(1.3)**	**88.6(1.2)**	**-93.7(1.0)**	**147.6(1.3)**	**61.3(7)**	**15.4(1.4)**	**-1.6(7)**	**14.7(1.9)**	**-0.4(1.3)**	**-12.3(6)**	
4	-120.1(1.3)	84.0(1.2)	-92.1(1.0)	145.9(1.3)	60.2(7)	15.0(1.4)	-1.5(7)	14.4(1.9)	-0.1(1.3)	-12.1(6)	
5	-112.0(9)	41.2(8)	-76.2(7)	127.5(9)	49.9(5)	11.6(9)	-0.4(5)	10.7(1.2)	1.8(8)	-10.2(4)	
6	-103.6(6)	11.2(5)	-63.9(5)	111.3(6)	42.0(3)	8.9(7)	0.2(3)	8.0(8)	2.6(6)	-8.6(3)	
7	-95.2(4)	-10.0(4)	-54.0(4)	97.1(4)	35.9(2)	6.9(5)	0.6(2)	6.0(6)	2.8(4)	-7.3(2)	
8	-87.1(3)	-24.9(3)	-46.1(3)	84.5(3)	31.0(2)	5.3(4)	0.7(2)	4.5(5)	2.7(3)	-6.1(2)	
$d_{\mathrm{Cu-Cu}}$ (Å)	2.992	3.000	3.165	3.287	3.453	4.567	4.673	4.674	4.700	4.968	

U eV	J_{11} (K)	J_{12} (K)	J_{13} (K)	J_{14} (K)	J_{15} (K)	J_{16} (K)	J_{17} (K)	J_{18} (K)	J_{19} (K)	J_{20}	θ_{CW} (K)
3.9	**-3.8(7)**	**6.4(1.1)**	**-0.6(1.2)**	**3.0(2.0)**	**-1.4(1.3)**	**-5.4(7)**	**-5.1(6)**	**14.6(6)**	**6.9(1.9)**	**12.6(1.1)**	**-34.7**
4	-3.8(7)	6.3(1.1)	-0.7(1.2)	3.0(2.0)	-1.3(1.3)	-5.3(7)	-5.0(6)	14.4(6)	6.8(1.9)	12.4(1.1)	-33.2
5	-3.5(5)	4.9(7)	-1.1(8)	3.0(1.3)	-0.7(9)	-4.1(4)	-3.8(4)	12.5(4)	5.4(1.2)	10.4(7)	-19.3
6	-3.0(3)	3.8(5)	-1.1(6)	2.8(9)	-0.3(6)	-3.2(3)	-2.9(3)	10.7(3)	4.3(8)	8.8(5)	-9.2
7	-2.4(2)	3.0(4)	-1.0(4)	2.5(6)	-0.1(4)	-2.5(2)	-2.1(2)	9.2(2)	3.4(6)	7.4(4)	-1.8
8	-1.9(2)	2.4(3)	-0.8(3)	2.2(5)	0.0(3)	-1.9(2)	-1.6(2)	7.8(2)	2.8(5)	6.2(3)	3.5
$d_{\mathrm{Cu-Cu}}$ (Å)	5.161	5.434	5.444	5.480	5.691	5.707	5.715	5.725	5.877	5.902	

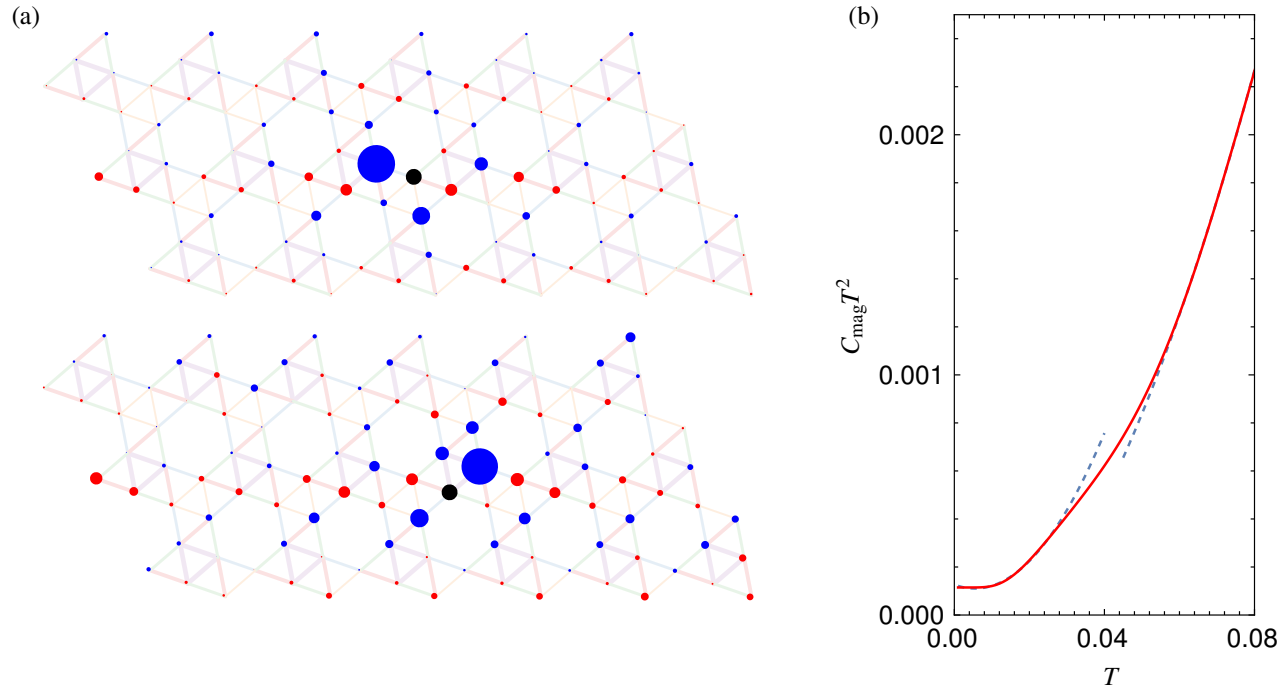

Figure S2. (a) The spin-spin correlation $\langle \vec{S}_j \cdot \vec{S}_r \rangle$ obtained from DMRG on a 108 site maple-leaf cluster. $\vec{S}_r$ is our reference spin which is marked in black. For the top panel we set $r = 63$ and for the bottom panel $r = 62$. The radius of the disks indicates the strength of the correlation and the color red (blue) indicates positive (negative) correlation. In both cases we see that in the bulk the spin-spin correlation decays very quickly, signalling a spin disordered ground state. (b) The $C_{\mathrm{mag}}T^2$ vs. T calculated via DMRG on a 48 site cluster. The calculations are done with 24 sweeps with a maximum bond dimension of 1024. Apart from the ground state, we also calculate 480 exited states to calculate the finite temperature properties. The dashed line is guide for the eye. One can see an anomalous behavior occurring at $\sim 0.04\widetilde{J} = 10$ K which is also seen in the experiments.

of the dominant coupling J_4. The couplings J_{11} to J_{14} and J_{17} are second neighbor couplings in the maple leaf lattice. They are at most 4% of the dominant coupling J_4.

Effective model.- As explained in the main text, the large ferromagnetic J_1 bonds of bluebellite lead to an effective spin-1 breathing kagome lattice behavior. In order to determine the exchange interactions of this effective model, we performed energy mapping in a $3\times1\times1$ supercell with 18 Cu sites where we constrained moments adjacent to the J_1 bond to be parallel. In this way, we determine the effective exchange interaction for the

Table S2. Crystal structure of bluebellite $Cu_6IO_3(OH)_{10}Cl$ with DFT optimized Cl, O and H positions. The lattice parameters of space group $R3$ (No. 146) were kept fixed at experimental values $a = 8.3056$ Å and $c = 13.2194$ Å [2].

atom	x	y	z
Cu1	0.4578	0.3867	0.2901
Cu2	0.0261	0.2404	0.2747
I	0.0000	0.0000	0.6050
O1	−0.244716	−0.154414	−0.120656
O2	0.000000	0.000000	0.249551
O3	0.190821	0.445737	0.171976
O4	−0.444508	−0.062377	0.031739
O5	0.412671	0.135042	0.022041
Cl	0.000000	0.000000	0.049719
H1	−0.260301	−0.167341	−0.197392
H2	0.000000	0.000000	0.172600
H3	−0.114255	−0.306030	−0.254043
H4	−0.454172	−0.185148	0.109447

spin-1 breathing kagome lattice. As shown in Fig. S1, we perform the energy mapping for five different U values. We use the same U value that is relevant for the original maple leaf lattice (see main text, Fig. 1) to determine the effective Hamiltonian parameters. The result is $J_{\rm eff} = 49(2)\,{\rm K}$, $J'_{\rm eff} = 18(2)\,{\rm K}$, $J^{\perp}_{1,\rm eff} = -2(3)\,{\rm K}$, $J^{\perp}_{3,\rm eff} = 1(2)\,{\rm K}$, $J_{2,\rm eff} = -3(2)\,{\rm K}$, $J'_{2,\rm eff} = 1(2)\,{\rm K}$. Due to the error bars, not so much information about the subleading couplings can be obtained. It is clear that the effective kagome lattice has only very small interlayer couplings $J^{\perp}_{i,\rm eff}$. The inplane second neighbor couplings on average appear to be slightly ferromagnetic.

II. DMRG METHODS AND RESULTS

The ground state energy of the bluebellite Hamiltonian, introduced in the main text, is calculated via DMRG using the ITENSOR [3] package. For the calculations, we use three different sized spin tubes with $N = 2$, 3, and 4 unit cells along the circumference of the tube. Along the length of the tube we always take $2N$ unit cells. Thus we do our calculations on $L = 2N^2 = 48, 108, 192$ site clusters. For $L = 48$ and 108, we perform 30 sweeps with a maximum bond dimension 2048. For $L = 192$ the number of sweeps was reduced to 24. The ground state energy obtained via these calculations is shown in the main text. We perform a linear fitting of the energies to obtain a finite size scaling. The spin-spin correlations from two central sites are shown in Fig. S2 (b). A fast decay of the long range spin-spin correlations is apparent there.

Next, to access the thermodynamic properties of the system, we calculate the magnetic specific heat by using the fundamental relation,

$$C_{\rm mag} \propto \frac{1}{LT^2}\left[\langle \hat{H}^2\rangle_{th} - \langle \hat{H}\rangle^2_{th}\right] \tag{S2}$$

where, T is the temperature of the system and $\langle \hat{Q}\rangle$ is the thermal average of an observable $\hat{Q}$, i.e.

$$\langle \hat{Q}\rangle_{th} = \frac{\sum_j \exp(-\beta E_j)\langle j|\hat{Q}|j\rangle}{\sum_j \exp(-\beta E_j)},$$

where β is the inverse temperature. This relation is easily derivable by taking the second derivative of the partition function

$$Z(\beta) = \sum_j \exp(-\beta E_j),$$

where the j sums runs over all the eigenenergies of the system. For practical calculations, we have to restrict ourselves to a finite number of lowest lying states $|j\rangle$ and their energies E_j known from DMRG. The corresponding expectation values $\langle j|\hat{H}|j\rangle$ and $\langle j|\hat{H}^2|j\rangle$ are E_j and E_j^2, respectively. For this part of the calculation we choose the 48 site cluster. We perform 24 sweeps with a maximum bond dimension of 512 and calculate the energies (E_j) of 481 lowest lying states. We estimate that for a L site cluster there will be $L/2$ strong singlets forming on the J_2 bonds. Each such singlet would have 3 excited triplet states. Therefore, we need more than $3L/2$ excited states to capture the finite temperature physics which will be missed by the bond-operator calculations. Thus it is an extremely costly calculation and also prone to numerical errors, and thus we only perform it on a small cluster to get an idea of the thermodynamic properties of the system which we show in Fig. S2 (c). We see an anomalous behavior occurring at ~ 10 K which becomes exceedingly pronounced with increasing number of excited states considered. We believe this comes from the thermal activation of the excited states that live above the triplets. This might also have a connection to the anomalous behavior seen in the experiments at 17 K.

III. DETAILS OF BOND-OPERATOR MEAN-FIELD THEORY

Based on our findings from the DMRG calculations of the Hamiltonian for bluebellite, we now develop an effective low-energy bosonic theory for various reasons. First we want to obtain an better understanding of the system at the thermodynamic limit. Secondly, such an approximate theory allows us to calculate static and dynamic spin structure factor of the system very easily. Additionally, we can gain some insight of the thermodynamic properties of the system as well.

Upon carefully observing the NN spin-spin correlations obtained from DMRG (See Fig. 1 of main text), we propose that a minimal low-energy physics of the system can be well described by assuming that the ground state of the system is a dimerized singlet with strong singlet weights on the J_2 bonds. To understand the effective low-energy physics of the system, we start with a $J_2 - J_3$ hexagon as our unit cell, and only consider the three

J_2 bonds as our elementary block,  , described by the Hamiltonian

$$\mathcal{H}_{\text{hex}} = J_2 \sum_{b=1,2,3} \left(\vec{S}_{2b-1} \cdot \vec{S}_{2b}\right) \tag{S3}$$

$$= J_2 \left(\vec{S}_1 \cdot \vec{S}_2 + \vec{S}_3 \cdot \vec{S}_4 + \vec{S}_5 \cdot \vec{S}_6\right), \tag{S4}$$

where $b = 1, 2, 3$ is the bond index (see Fig.S3). The ground state of this Hamiltonian is a product state of singlets forming on the 1-2, 3-4, and 5-6 spin pairs, which allows us to use the bond-operator formalism [4] to represent the spin operators as

$$S^{\alpha}_{2b-1} = -\frac{1}{2}\left(\hat{s}_b \hat{t}^{\alpha\dagger}_b + \hat{s}^{\dagger}_b \hat{t}^{\alpha}_b\right) \tag{S5a}$$

$$S^{\alpha}_{2b} = \frac{1}{2}\left(\hat{s}_b \hat{t}^{\alpha\dagger}_b + \hat{s}^{\dagger}_b \hat{t}^{\alpha}_b\right). \tag{S5b}$$

In writing the above representation, one makes use of the basis of the singlet, $|s_b\rangle$, and three triplets, $|t^{\pm 1,0}_b\rangle$, defined on the bond b. On a Fock space with vaccum, $|\varnothing\rangle_b$, the singlet and the triplet operators are defined as

$$|s_b\rangle = \hat{s}^{\dagger}_b |\varnothing\rangle_b \tag{S6a}$$

$$|t^m_b\rangle = \hat{t}^{m\dagger}_b |\varnothing\rangle_b, \tag{S6b}$$

with $\hat{s}_b$ and $\hat{t}^m_b$ being bosonic operators. A boson number constraint

$$\hat{s}^{\dagger}_b \hat{s}_b + \sum_{m=-1,0,1} \hat{t}^{m\dagger}_b \hat{t}^m_b = 1 \tag{S7}$$

must also be satisfied on every bond. In terms of the singlet and he triplet operators defined above $\mathcal{H}_{\text{hex}}$ reads as,

$$\mathcal{H}_{\text{hex}} = -\frac{3}{4} J_2 \sum_b \hat{s}^{\dagger}_b \hat{s}_b + \frac{1}{4} J_2 \sum_b \sum_{\alpha=x,y,z} \hat{t}^{\alpha\dagger}_b \hat{t}^{\alpha}_b \tag{S8}$$

where

$$\hat{t}^{x\dagger} = \frac{1}{\sqrt{2}}\left(\hat{t}^{-1\dagger}_b - \hat{t}^{1\dagger}_b\right) \tag{S9a}$$

$$\hat{t}^{y\dagger} = \frac{i}{\sqrt{2}}\left(\hat{t}^{-1\dagger}_b + \hat{t}^{1\dagger}_b\right) \tag{S9b}$$

$$\hat{t}^{z\dagger} = \hat{t}^{0\dagger}_b. \tag{S9c}$$

Next, we rewrite our full Hamiltonian and recast it in terms of the "coordinate" operator

$$\hat{Q}^{\alpha}_b = \frac{1}{\sqrt{2}}\left(\hat{t}^{\alpha\dagger}_i + \hat{t}^{\alpha}_i\right) \tag{S10}$$

and its conjugate momentum operator

$$\hat{P}^{\alpha}_b = \frac{i}{\sqrt{2}}\left(\hat{t}^{\alpha\dagger}_i - \hat{t}^{\alpha}_i\right). \tag{S11}$$

Thus, the final form of the full Hamiltonian, $\mathcal{H}$, on N_{uc} unit-cells reads as,

$$\mathcal{H} \approx \mathcal{H}_{\text{MF}} = e_0 N_{\text{uc}} + \frac{1}{2} \sum_{\mathbf{k}} \sum_{\alpha} \left[\lambda \hat{\mathbf{P}}^{\alpha\dagger}_{\mathbf{k}} \hat{\mathbf{P}}^{\alpha}_{\mathbf{k}} + \hat{\mathbf{Q}}^{\alpha\dagger}_{\mathbf{k}} \mathcal{V}^{\alpha}_{\mathbf{k}} \hat{\mathbf{Q}}^{\alpha}_{\mathbf{k}}\right]. \tag{S12}$$

Here, $e_0 = -3J_2\bar{s}^2 + \frac{3}{4}J_2 + 3\lambda\bar{s}^2 - \frac{15}{2}\lambda$, with $\bar{s}$ being the mean singlet amplitude on all the J_2 bonds. λ is the Lagrange multiplier used to satisfy the boson number constraint in (S7) on average.

$$\hat{\mathbf{P}}^{\alpha\dagger}_{\mathbf{k}} = \begin{bmatrix} \hat{P}^{\alpha\dagger}_{1\mathbf{k}} & \hat{P}^{\alpha\dagger}_{2\mathbf{k}} & \hat{P}^{\alpha\dagger}_{3\mathbf{k}} \end{bmatrix} \tag{S13}$$

$$\hat{\mathbf{Q}}^{\alpha\dagger}_{\mathbf{k}} = \begin{bmatrix} \hat{Q}^{\alpha\dagger}_{1\mathbf{k}} & \hat{Q}^{\alpha\dagger}_{2\mathbf{k}} & \hat{Q}^{\alpha\dagger}_{3\mathbf{k}} \end{bmatrix} \tag{S14}$$

and

$$\mathcal{V}^{\alpha}_{\mathbf{k}} = \begin{bmatrix} \lambda & \eta_{12} & \eta^*_{31} \\ \eta^*_{12} & \lambda & \eta_{23} \\ \eta_{31} & \eta^*_{23} & \lambda \end{bmatrix} \tag{S15}$$

with

$$\eta_{12} = \frac{\bar{s}^2}{2}\left[-J_3 + (J_5 - J_1)e^{i\mathbf{k}\cdot\mathbf{a_2}} + J_4 e^{i\mathbf{k}\cdot\mathbf{a_1}}\right] \tag{S16a}$$

$$\eta_{23} = \frac{\bar{s}^2}{2}\left[-J_3 + (J_5 - J_1)e^{-i\mathbf{k}\cdot\mathbf{a_1}} + J_4 e^{-i\mathbf{k}\cdot(\mathbf{a_1}-\mathbf{a_2})}\right] \tag{S16b}$$

$$\eta_{31} = \frac{\bar{s}^2}{2}\left[-J_3 + (J_5 - J_1)e^{i\mathbf{k}\cdot(\mathbf{a_1}-\mathbf{a_2})} + J_4 e^{-i\mathbf{k}\cdot\mathbf{a_2}}\right]. \tag{S16c}$$

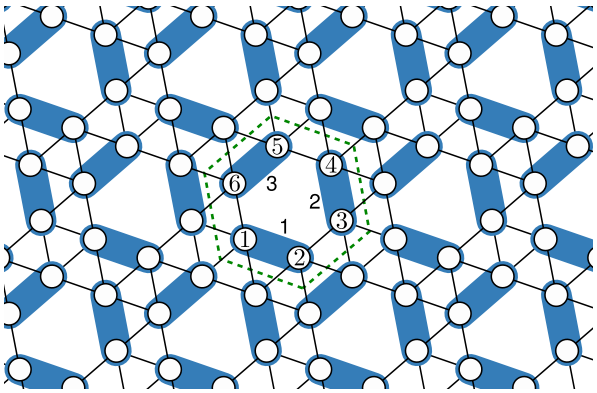

Figure S3. The singlet product state used in our bond-operator mean-field calculation. The singlets are forming on the J_2 bonds. We use the dashed green hexagon as our unit cell, which contains three symmetry related dimers. The indexing of the bonds and the sites in the unit cell are also marked.

(the lattice vectors $\mathbf{a}_1 = \sqrt{7}/2(\hat{x} + \sqrt{3}\hat{y})$ and $\mathbf{a}_2 = \sqrt{7}\hat{x}$). Moreover, $\hat{P}^{\alpha\dagger}_{b\mathbf{k}}$'s and $\hat{Q}^{\alpha\dagger}_{b\mathbf{k}}$'s are the Fourier components of $\hat{P}^{\alpha\dagger}_{b}(\mathbf{r})$'s and $\hat{Q}^{\alpha\dagger}_{b}(\mathbf{r})$'s, respectively, i.e. $\hat{P}^{\alpha\dagger}_{b\mathbf{k}} = 1/\sqrt{N_{\rm uc}}\sum_{\mathbf{k}} e^{i\mathbf{k}\cdot\mathbf{r}}\hat{P}^{\alpha\dagger}_{b}(\mathbf{r})$ and $\hat{Q}^{\alpha\dagger}_{b\mathbf{k}} = 1/\sqrt{N_{\rm uc}}\sum_{\mathbf{k}} e^{i\mathbf{k}\cdot\mathbf{r}}\hat{Q}^{\alpha\dagger}_{b}(\mathbf{r})$.

$\mathcal{H}_{\rm MF}$ now is a problem of three coupled differential equations, which one diagonalizes to obtain

$$\mathcal{H}_{\rm MF} = e_0 N_{\rm uc} + \sum_m \sum_{\mathbf{k}} \sum_{\alpha} \omega^{\alpha}_{\mathbf{k},m} \left(\gamma^{\alpha\dagger}_{\mathbf{k},m}\gamma^{\alpha}_{\mathbf{k},m} + \frac{1}{2} \right) \tag{S17}$$

where $\gamma^{\alpha}_{\mathbf{k},m}$ are renormalized triplon operators, and

$$\omega^{\alpha}_{\mathbf{k},m} = \sqrt{\lambda\left(\lambda - \frac{1}{2}\bar{s}^2\xi^{\alpha}_{\mathbf{k},m}\right)} \tag{S18}$$

with

$$\xi^{\alpha}_{\mathbf{k},m} = 2\sqrt{-\frac{p_{\mathbf{k}}}{3}}\cos\left[\frac{1}{3}\cos^{-1}\left(\frac{3q_{\mathbf{k}}}{2p_{\mathbf{k}}}\sqrt{-\frac{3}{p_{\mathbf{k}}}} - \frac{2\pi}{3}m\right)\right] \tag{S19}$$

and

$$p_{\mathbf{k}} = -\left(|\eta_{12}|^2 + |\eta_{23}|^2 + |\eta_{31}|^2\right) \tag{S20}$$

$$q_{\mathbf{k}} = 2\mathrm{Re}\left(\eta_{12}\eta_{23}\eta_{31}\right). \tag{S21}$$

The ground state of the system is given by the vaccum of the quasi-particles, $\gamma^{\alpha}_{\mathbf{k},m}$, i.e., the ground state energy per site of the system is given by,

$$e_g = \frac{e_0}{6} + \frac{1}{12N_{\rm uc}}\sum_m\sum_{\mathbf{k}}\sum_{\alpha}\omega^{\alpha}_{\mathbf{k},m} \tag{S22}$$

The unknown mean-field parameters, λ and $\bar{s}^2$ are determined by minimizing e_g, which leads to the following self-consistent equations

$$\lambda = J_2 + \frac{1}{12N_{\rm uc}}\sum_m\sum_{\mathbf{k}}\sum_{\alpha}\frac{\lambda\xi^{\alpha}_{\mathbf{k},m}}{2\omega^{\alpha}_{\mathbf{k},m}} \tag{S23a}$$

$$\bar{s}^2 = \frac{5}{2} - \frac{1}{12N_{\rm uc}}\sum_m\sum_{\mathbf{k}}\sum_{\alpha}\frac{4\lambda - \bar{s}^2\xi^{\alpha}_{\mathbf{k},m}}{2\omega^{\alpha}_{\mathbf{k},m}}. \tag{S23b}$$

To access finite temperature properties from the bond-operator mean-field theory we employ the methodology used by Normand *et. al.* [5]. First of all, a full thermal occupation function of hard–core bosons is impossible to obtain because of the exclusion constraint of (S7). It can, however, be approximated via a statistical reweighting of the free-boson numbers [6], i.e. suppressing the magnon density of states for all magnon sectors – the more magnons in a sector, the stronger the suppression. This leads to the effective single-dimer free energy

$$f = -\frac{1}{\beta}\ln\left[1 + \sum_{m,\alpha} z_{m,\alpha}(\beta)\right] \tag{S24}$$

where

$$z_{m,\alpha}(\beta) = \frac{1}{N_{uc}}\sum_{\mathbf{k}}\exp\left(-\beta\omega^{\alpha}_{\mathbf{k},m}\right)$$

is the partition function of the triplet t^{α}_{m}. The effective statistics obtained from such a statistical ansatz are given by,

$$n(\omega^{\alpha}_{\mathbf{k},m},\beta) = \frac{\exp\left(-\beta\omega^{\alpha}_{\mathbf{k},m}\right)}{1 + \sum_{m,\alpha} z_{m,\alpha}(\beta)}, \tag{S25}$$

where β is the inverse temperature [7]. The magnetic specific heat, hereafter, is easily derived by taking a second derivative of the free-energy with respect to temperature. The magnetic specific heat thus obtained reads as,

$$C_{\rm mag}(\beta) = \sum_{m,\mathbf{k},\alpha}\left[\frac{\left(\beta\omega^{\alpha}_{\mathbf{k},m}\right)^2\exp\left(-\beta\omega^{\alpha}_{\mathbf{k},m}\right)}{1 + \frac{1}{N_{uc}}\sum_{m,\mathbf{k},\alpha}\exp\left(-\beta\omega^{\alpha}_{\mathbf{k},m}\right)} - \left\{\frac{\beta\omega^{\alpha}_{\mathbf{k},m}\exp\left(-\beta\omega^{\alpha}_{\mathbf{k},m}\right)}{1 + \frac{1}{N_{uc}}\sum_{m,\mathbf{k},\alpha}\exp\left(-\beta\omega^{\alpha}_{\mathbf{k},m}\right)}\right\}^2\right]. \tag{S26}$$

The results obtained from the finite temperature calculations are depicted in Fig. 3 of the main text.

IV. LUTTINGER-TISZA ANALYSIS OF THE BLUEBELLITE

The full model Hamiltonian of bluebellite is not amenable to a solution in the classical, i.e. $S \to \infty$ limit, where spin operators are replaced by vector spins. Therefore, we resort to the Luttinger-Tisza approximation [8, 9], where the normalization of the spins is enforced only on average, allowing for analytical solution of the model. The corresponding band-structure in Fig. S4 shows a flat lowest band with a band-with of 4% of $\tilde{J}$, and an almost degenerate area around the Γ point, featuring soft minima along the Γ–M direction. While in the classical limit, even in the Luttinger-Tisza approximation,

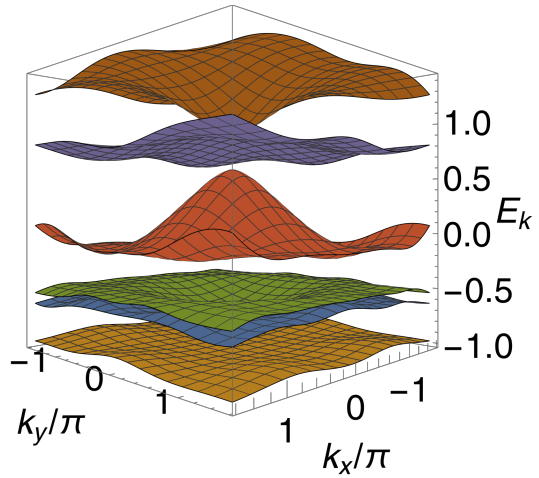

Figure S4. Luttinger-Tisza band-structure of the full bluebellite model Hamiltonian. The lowest band has a width of of 4% of $\tilde{J}$ with soft minima along the Γ–M direction within an almost flat area around the origin in reciprocal space.

this energy landscape implies an ordered ground state, quantum fluctuations can access these low-lying states by allowing for variations in the spin expectation values. Therefore, the flatness of the lowest Luttinger-Tisza band indicates the probability for the quantum model to avoid long-range order, as we find for bluebellite.

[1] S. J. Mills, A. R. Kampf, A. G. Christy, R. M. Housley, G. R. Rossman, R. E. Reynolds, and J. Marty, Bluebellite and mojaveite, two new minerals from the central Mojave Desert, California, USA, Mineralog. Mag. **78**, 1325–1340 (2014).

[2] Y. Haraguchi, A. Matsuo, K. Kindo, and Z. Hiroi, Quantum antiferromagnet bluebellite comprising a maple-leaf lattice made of spin-1/2 Cu^{2+} ions, Phys. Rev. B **104**, 174439 (2021).

[3] M. Fishman, S. R. White, and E. M. Stoudenmire, The ITensor Software Library for Tensor Network Calculations, SciPost Phys. Codebases , 4 (2022).

[4] S. Sachdev and R. N. Bhatt, Bond-operator representation of quantum spins: Mean-field theory of frustrated quantum Heisenberg antiferromagnets, Phys. Rev. B **41**, 9323 (1990).

[5] B. Normand and C. Rüegg, Complete bond-operator theory of the two-chain spin ladder, Phys. Rev. B **83**, 054415 (2011).

[6] M. Troyer, H. Tsunetsugu, and D. Würtz, Thermodynamics and spin gap of the heisenberg ladder calculated by the look-ahead lanczos algorithm, Phys. Rev. B **50**, 13515 (1994).

[7] C. Rüegg, B. Normand, M. Matsumoto, C. Niedermayer, A. Furrer, K. W. Krämer, H.-U. Güdel, P. Bourges, Y. Sidis, and H. Mutka, Quantum statistics of interacting dimer spin systems, Phys. Rev. Lett. **95**, 267201 (2005).

[8] D. H. Lyons and T. A. Kaplan, Method for determining ground-state spin configurations, Phys. Rev. **120**, 1580 (1960).

[9] T. A. Kaplan and N. Menyuk, Spin ordering in three-dimensional crystals with strong competing exchange interactions, Phil. Mag. **87**, 3711 (2007).